AIAA JOURNAL
Vol. 35, No. 2, February 1997

Overlay Method for Calculating Excited State Species Properties in Hypersonic Flows

Deborah A. Levin*
Institute for Defense Analyses, Alexandria, Virginia 22311-1772
and
Graham V. Candler† and Robert J. Collins‡
University of Minnesota, Minneapolis, Minnesota 55455

In many hypersonic flows, the excited states of some chemical species are the dominant radiators. Often, those electronically excited particles are present in small concentrations and the chemical kinetics mechanisms for their formation are very complicated and costly to implement in a fully coupled computational fluid dynamics method. An efficient computational method is presented for the calculation of chemical species present in trace amounts, including excited state species. The usefulness of this overlay method is demonstrated with several examples: OH(A) formation from water vapor in a hypersonic shocklayer, state-specific CO vibrational relaxation and CO(a) formation in a rocket motor nozzle, and CO(a) kinetics in an expanding flow. The overlay calculations allow a careful sensitivity analysis of the kinetics modeling and permit comparison with radiance data obtained in flight.

Introduction

THERE has been a general interest within the hypersonics community to study optical emissions from chemically reacting flows in nonequilibrium. Such radiation can be measured in both ground-based and flight experiments with well-established instrumentation techniques. These measurements provide data to validate the modeling of species concentrations and temperatures in hypersonic flows.

The approach commonly used today to model the spectral radiant intensity for different flow conditions is to first obtain a solution to the conservation equations for species concentrations and temperatures as a function of their location in the flow. An important aspect of the flow modeling is that the chemical kinetics model applies to the ground-state species only. Then a separate radiation model uses the flow solution to compute the spectral radiance at each point in the flow. The radiation model generally consists of two parts: computation of the excited state species concentrations and the line-by-line spectral distribution of the radiation. Usually, the first part of the model has the greater degree of uncertainty.

To calculate the excited state populations, one typically assumes a master set of rate equations for populating the excited state levels. For the calculation of radiation in the ultraviolet to visible spectral region, these equations represent the distribution of excited states in the atomic or molecular vibrational, rotational, and electronic levels. When the collision rate is sufficiently high, it is also assumed that the excited state population distribution is the quasi-steady-state (QSS) solution of the master set of equations. This condition occurs if two criteria are met. First, the time constants for the population excitation equations must be fast compared with the average gas flow residence time. Second, the production and destruction rates are closely balanced.[1] The QSS condition has been found to hold for the population of the electronic states of NO for stagnation region flows for 10-cm-radius spheres at a speed of 5 km/s and up to altitudes of 80 km (Ref. 2). However, there are other situations where it is expected to fail.

The second assumption usually made in the solution of the master equations for the excited state populations is that the primary creation mechanism is by electron or neutral collisions with the ground-state species. As the flow density decreases, collisions between two ground-state species that directly produce the excited state species become important. These chemiluminescent reactions are known to be potentially important for the two cases that we present here.

The addition of excited state mechanisms to the reaction set increases the computational cost of the flow solution. In rarefied conditions, many reaction paths are possible and must be included. Often the rate constants and branching ratios are not well known. For these reasons, multiple computations are often required to quantify the sensitivity of the inclusion or exclusion of specific processes and the uncertainty in the rate constants.

Hence, an efficient computational method is required to calculate the electronically excited states in both compressed and expanding flows. A method is presented, based on the key assumption that the excited electronic state species concentrations are sufficiently small such that they are trace species compared with the bulk flow. Then, an example calculation of the concentration of electronically excited hydroxyl radicals, OH(A), in a stagnation region flow is considered. This calculation can be compared directly with the conventional, uncoupled approach. This comparison provides the validation of the method.

The second example corresponds to the calculation of the excited state CO(a) population in an expanding flow from a solid rocket motor. This problem cannot be solved in the uncoupled manner because the long lifetime of the CO(a) state and the low collision frequency in the expanding flow make the use of the QSS approximation questionable. The large number of reactions and processes that need to be considered will illustrate the efficiency and usefulness of the proposed technique. This case requires a description of the ground-state chemical two-phase flow. There exists a wealth of detailed modeling of rocket motor operation and nozzle exhaust properties that has been primarily focused on evaluating motor performance. The results of this modeling must be taken into consideration as one tries to model the radiation due to plume–freestream interactions. Modification of these models to directly include excited state chemistry is not straightforward. Therefore, a method that utilizes well-developed, two-phase flow packages[3,4] as the basis for modeling excited state chemistry unifies separate research communities. Moreover, it enables the use of optical diagnostics as a tool for the understanding of motor operation and plume radiance in the ultraviolet.

Flowfield Simulation Method

The overlay method that we describe in this work consists of two steps. First, the flowfield is simulated by solving the Navier–Stokes

Received April 27, 1996; revision received Oct. 16, 1996; accepted for publication Oct. 25, 1996; also published in *AIAA Journal on Disc*, Volume 2, Number 2.

*Research Staff Member, Science and Technology Division. Member AIAA.
†Associate Professor, Department of Aerospace Engineering and Mechanics. Member AIAA.
‡Professor Emeritus, Department of Electrical Engineering.

equations that have been extended to include the effects of finite rate chemical reactions and internal energy relaxation. This solution includes all of the chemical species that may be present in large amounts or those that are important in the chemical kinetics of those major species. Then, the mass conservation equations for the trace chemical species are overlaid on the previously computed flowfield. Because the trace species are present in very small amounts, they do not affect the mass, momentum, or energy of the bulk flow.

The computational fluid dynamics method that was used to simulate the flow of the major species in the stagnation region of a re-entry experiment[5] and in the plume of the thrusting rocket[6] has been discussed in earlier work. The baseline model for air is a reacting mixture of thermally perfect gases composed of the following chemical species: N_2, O_2, NO, N, and O. These species are allowed to react with one another at finite rates. Here NO is included as a major species because it may be present in relatively large amounts and because is acts as a reaction intermediary in the Zeldovich reactions. The internal energy is described by translational, rotational, and vibrational temperatures. Finite rate relaxation of the rotational and vibrational temperatures to the translational temperature is also modeled.

The flow is assumed to be described by the extended Navier–Stokes equations, which for two-dimensional flows may be written in conservation law form as

$$\frac{\partial \boldsymbol{U}}{\partial t} + \frac{\partial \boldsymbol{F}}{\partial x} + \frac{\partial \boldsymbol{G}}{\partial y} = \boldsymbol{W} \tag{1}$$

where $\boldsymbol{U}$ is the vector of conserved quantities, $\boldsymbol{F}$ and $\boldsymbol{G}$ are the flux vectors in the x and y directions, respectively, and $\boldsymbol{W}$ is the source vector due to chemical reactions and the relaxation of the vibrational and rotational temperatures toward the translational temperature. More details concerning the form of the fluxes and the source vector may be found in earlier work.[5] The numerical method for the solution of Eq. (1) uses modified Steger–Warming flux vector splitting,[7] and the steady-state solution is obtained using implicit Gauss–Seidel linerelaxation.[8] The method has been validated by comparison to a wide range of experimental data. The flow properties thus obtained will be hereafter referred to as the bulk solution.

If the argument is made that the introduction of trace species into the bulk flow does not affect the energy or momentum of the bulk solution, then a simplified conservation law for these overlay species can be written

$$\frac{\partial \rho_s}{\partial t} + \frac{\partial}{\partial x}(\rho_s u + \rho_s \hat{u}_s) + \frac{\partial}{\partial y}(\rho_s v + \rho_s \hat{v}_s) = w_s$$

$$s = 1, 2, \ldots, n_s \tag{2}$$

where s is the index of each of the n_s overlay species, ρ_s is the species mass density, w_s is the chemical source term, u and v are the mass-averaged flow velocities in the x and y directions, and $\hat{u}_s$ and $\hat{v}_s$ are the diffusion velocities of species s. The mass-averaged velocities are obtained from the bulk solution, as are the densities of the major species and the temperatures that appear in the chemical source term. Hence, once the steady-state bulk solution has been obtained, Eq. (2) can be solved. Note that the overlay approach could also be used to add internal energy conservation equations, provided that the energy contained in these modes is small compared with the total energy; however, this approach has not been employed to date.

To make this decomposition of the flowfield into a bulk solution and an overlay solution, we have assumed that the overlay species do not alter the state of the bulk solution appreciably. There are three criteria that must be met for this condition to hold. First, the trace species must be present in small amounts so that only a small fraction of the mass is missing from the bulk flow solution. Second, the presence of the trace species cannot affect the diffusion coefficients of the bulk species. A very light overlay species, such as H, could possibly alter the mass diffusion coefficient of the heavy bulk species if it was present in large mass fractions. However, as the overlay species are present in only trace amounts, this is not an important effect. Third, and most importantly, the overlay species cannot affect the chemical kinetics of the bulk species. For example, NO may be present in only small amounts, but it may be the most efficient reaction path for the dissociation of N_2. Therefore, it cannot be treated as an overlay species unless N_2 dissociation is not important under the conditions of the simulation. In practice, with the appropriate choice of the overlay species, we can apply this method when the trace species are present at levels of less than about 10^{-4} mass fraction, which would produce errors of less than 0.1% in the bulk solution properties.

The overlay equations, Eq. (2), must be solved in an analogous fashion to the bulk solution, Eq. (1). That is, the same numerical method must be used so that mass conservation of the trace species is assured. Also, for simplicity and to reduce interpolationerrors, the overlay solution is obtained on the same grid as the bulk solution. The numerical method for the overlay equations may be derived in a similar fashion to the method for the bulk solution. We recognizethat the convective fluxes are homogeneous in the conserved quantities. For example, the convective flux vector in the x direction is

$$\boldsymbol{F}_s = \begin{pmatrix} \rho_1 u \\ \rho_2 u \\ \vdots \\ \rho_{n_s} u \end{pmatrix} = A\boldsymbol{U}_s = u I \boldsymbol{U}_s \tag{3}$$

where $\boldsymbol{U}_s$ is the vector of conserved quantities, $U_s = (\rho_1, \rho_2, \ldots, \rho_{n_s})t$, and I is the $n_s \times n_s$ identity matrix. It is straightforward to develop an upwind differencing method where the direction of differencing is based on the sign of u. However, this could lead to a mismatch between the bulk and trace species solutions at discontinuities. Rather, the same method that is used to compute the u-convection speed in the bulk solution should be used in this calculation as well.

For example, in our calculations, we use a modified Steger–Warming flux-vector-splittingapproach, where for first-order accuracy, the $i+\frac{1}{2}$ cell-face split fluxes, $\boldsymbol{F}^+_{si+1/2}$ and $\boldsymbol{F}^-_{si+1/2}$, are computed using

$$\boldsymbol{F}^+_{si+\frac{1}{2}} = A^+_{i+\frac{1}{2}} \boldsymbol{U}_{si} \qquad \boldsymbol{F}^-_{si+\frac{1}{2}} = A^-_{i+\frac{1}{2}} \boldsymbol{U}_{si+1} \tag{4}$$

and

$$A^{\pm}_{i+\frac{1}{2}} = A^{\pm}\left[\tfrac{1}{2}(\boldsymbol{U}_i + \boldsymbol{U}_{i+1})\right] \tag{5}$$

The split Jacobian matrices $A^{\pm}$ are simply given by $A^{\pm}(\boldsymbol{U}) = \frac{1}{2}(u \pm |u|)I$ or with the modification suggested by Buning and Steger[9] to correct the slope discontinuity in stagnation regions. In regions of strong pressure gradients, we smoothly switch to true Steger–Warming flux vector splitting. Then the x direction split fluxes are

$$\boldsymbol{F}^+_{si+\frac{1}{2}} = A^+_i \boldsymbol{U}_{si} \qquad \boldsymbol{F}^-_{si+\frac{1}{2}} = A^-_{i+1} \boldsymbol{U}_{si+1} \tag{6}$$

The switching between the two upwind flux representations must be done in the same way in the overlay solution as in the bulk flow solution.

The solution of Eq. (2) is much less costly than the solution of Eq. (1) would be if both the bulk and overlay species were included. This is because the cost of solving Eqs. (2) and (1) scale approximately as the square of the number of equations being solved. By solving two smaller sets of equations, the computational cost is reduced. Also, aside from the source terms, Eq. (2) is linear in ρ_s, making it easier to solve. Also note that the flux vector splitting is dramatically simplified because the flux Jacobian is a diagonal matrix, and therefore the evaluation of the fluxes is trivial. Also, many of the components of the source terms can be computed once and stored for use in all subsequenttime steps during convergenceto steady state. Therefore, the cost per iteration of the overlay equations is considerably less than that of the full equation set. In practice, the overlay equation set usually converges to a steady state with about a factor of 10 fewer iterations than the bulk solution. Thus, it is possible to incorporate detailed excited state chemistry models in the overlay solution. Moreover, for altitude regimes where the continuum formulation becomes questionable, Eq. (2) can be solved relative to the bulk flow properties derived from a direct simulation Monte Carlo (DSMC) solution[10] and, if necessary, using mass diffusion properties computed with the DSMC method.

Modeling of the OH(*A*) Population in the Bow Shock Flow

Our analyses of the bow shock ultraviolet (BSUV) flights 1 and 2 have identified the modeling of radiation from the OH(A) state as important for understanding ultraviolet molecular radiation in transitional flows.[11] We have tested the validity of the overlay method for the production of the ground-state trace species of water, H, and OH by comparison with fully coupled calculations. Once the five-species reacting air calculation was obtained, the overlay solution cost was almost negligible (less than 10% of the bulk solution). The processes considered in this work for the formation of OH(A) are added to the ground-state processes used in our earlier work.[11] They are

$$O_2 + H \underset{}{\overset{k_1}{\longleftrightarrow}} O + OH \tag{7}$$

$$H_2O + N_2 \underset{}{\overset{k_2}{\longleftrightarrow}} OH + H + N_2 \tag{8}$$

$$OH + N_2 \underset{}{\overset{k_3}{\longleftrightarrow}} O + H + N_2 \tag{9}$$

$$H_2O + O \xrightarrow{k_{4f}} 2OH \tag{10}$$

$$H + O + M \xrightarrow{k_{5f}} OH(A) + M \tag{11}$$

$$H + 2OH \xrightarrow{k_{6f}} H_2O + OH(A) \tag{12}$$

$$OH(A) + M \underset{}{\overset{k_7}{\longleftrightarrow}} OH + M,\ M = N_2, O_2 \tag{13}$$

$$OH(A) \xrightarrow{A} OH(X) + h\nu \tag{14}$$

where M is a neutral third body, most likely N_2. Table 1 (Refs. 12–15) gives the Arrhenius parameter values assumed for the rates in Eqs. (7–14).

Figure 1 shows a plot of the number density as a function of distance from the wall along the stagnation streamline for the hydrogenated ground state and OH(A) excited state species. The overlay calculations were performed for a sphere cone with a 4-in. nose radius, at a velocity of 5 km/s and an altitude of 85 km. It is assumed that the water dissociation rate is governed by the translational temperature, which reaches a peak value of about 13,000 K in the stagnation region. The ground-state hydrogenated species are present in concentrations of about four orders of magnitude less than the freestream number density.

Table 1 OH (*A*) excitation model[a,b]

Equation no.	C_{fi}	η_i	E_{fi}/R	Source
7	2.2×10^{14}	0.0	16,646.0	Baulch et al.[12]
8	3.5×10^{16}	0.0	100,510.0	Baulch et al.[12]
9	7.5×10^{14}	0.06	100,470.0	Baulch et al.[12]
10	6.8×10^{13}	0.0	9,240.0	Baulch et al.[12]
11	1.2×10^{13}	0.0	6,940.0	Hidaka et al.[13]
12	8.3×10^{15}	0.0	0.0	Davis et al.[14]
13, $M = N_2$	4.2×10^{8}	0.5	−687.0	Copeland et al.[15]
13, $M = O_2$	4.6×10^{9}	0.5	−450.0	
14	1.4×10^{6}	0.0	0.0	Copeland et al.[15]

[a] $k_{if} = C_{fi} T^{\eta_i} \exp(-E_{fi}/RT)$.
[b] The units of the rates are in cm^3/mole/s (or higher), $R = 1.9872$ cal/mole-K, and E_{fi} is in cal/mole.

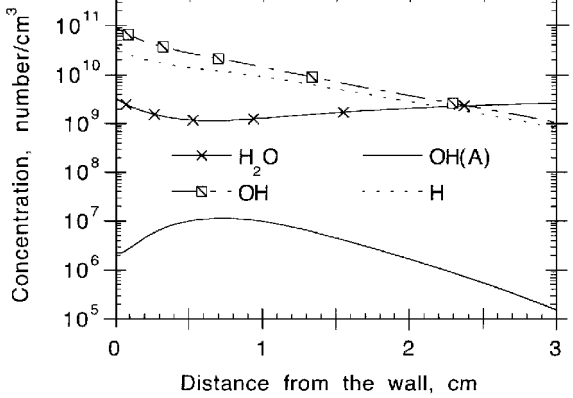

Fig. 1 OH(*A*) and hydrogenated species.

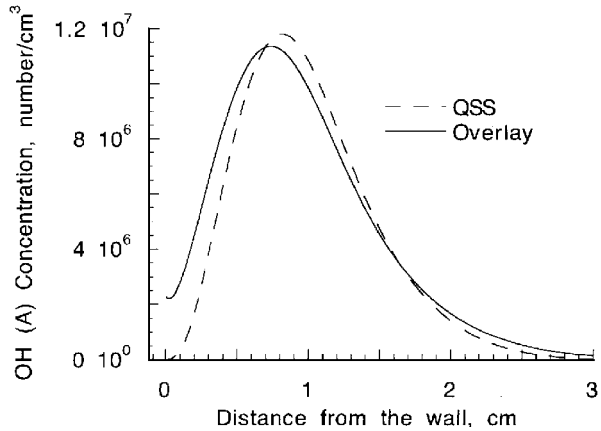

Fig. 2 Comparison of modeled OH(*A*) state populations on the stagnation streamline obtained from the QSS and overlay methods.

Figure 2 shows a comparison of the OH(A) concentration in the stagnation streamline obtained by the overlay technique (Fig. 1) and that obtained by solution of the QSS equations in the radiation-excitation model. The overlay method and the QSS distribution produce similar profiles of OH(A) across the shock layer. However, note that the overlay result is shifted slightly downstream toward the body surface, its peak is reduced in magnitude, and it predicts more OH(A) near the body surface. These three effects occur due to the correct nonequilibrium formation of OH(A) in this shock layer. At lower densities or in regions where the gas velocity is higher, these effects would be increased and the QSS distribution would be in error. The integrated number density through the shock layer of the OH(A) concentration obtained with the overlay and the QSS methods are 1.4×10^7 and $1.3 \times 10^7/cm^2$, respectively. Because the shock layer radiance is directly proportional to this quantity, the small difference between the two methods is insignificant for this case. The same level of agreement between the overlay and the QSS OH(A) integrated number density was obtained for the spherical region of the sphere cone shape.

The agreement between the QSS and overlay result is physically reasonable, even at an altitude of 85 km. Although the flow is highly rarefied, the production of OH(A) is dominated by Eqs. (8), (13), and (14). The collision rates are still sufficiently high such that these rates are fast compared with the flow residence time in the stagnation region. Earlier work with the same vehicle shape and velocity[2] verified this result for the NO(A) state population at 80 km. Because OH($A \rightarrow X$) and NO($A \rightarrow X$) are strong dipole allowed transitions the OH(A) QSS overlay comparison applies to both systems. However, the computational method used in earlier work[2] could not be extended to more rarefied flows or a two-dimensional calculation.

Modeling of the CO(*a*) Population in a Plume Flow

The second example involves the modeling of the population of a relatively long-lived electronically excited state, CO(a), which radiates to the ground state to produce the Cameron bands. In particular, we are interested in using the overlay technique to model the plume radiance that was observed from two solid-propellant motors at about 100 km altitude. The substantial increase in the lifetime of this state, compared with the first example, and the large number of reaction mechanisms necessitate the use of the overlay technique.

In addition to demonstrating the utility of the overlay technique, there is an additional motivation for selecting this case. The observation of the Cameron band emission from the Antares and Star-27 rocket engine was unexpected because molecular emission from solid propellants had never been observed before. In the work of Candler et al.[6] the presence of this radiation was noted, but its origin

was not explained. Hence the principal use of the overlay technique in this work is to explore, for the first time, different sources of this radiation in a quantitative manner.

We consider two basic classes of reaction mechanisms as the source of the radiation. Because the combustion process of the Antares (and Star-27) motors produces a gas with about 40% mole fraction of CO, we examine the likelihood that a sufficient amount in the $a^3\Pi$ excited state is produced in the combustion chamber and exits the motor nozzle. If the excited state CO population freezes, then the external flow conditions are sufficiently rarefied so that further electronic state quenching is unlikely. The second class of mechanisms tests the possibility of producing a sufficient amount of CO($a^3\Pi$) to explain the observed radiation by excitation of nozzle exit species with the plume–body shock layer. In both cases we have assumed that all excitation mechanisms are gas phase; i.e., the micron-sized solid alumina particles do not directly provide a source of reactants or surface reaction sites during the excitation processes.

We start with the first class of reaction mechanisms, hereafter referred to as the internal nozzle set. To calculate the CO(a) state profile in the nozzle we need to know the concentrations of the major ground-state chemical species of an aluminized solid propellant and the gas temperature as the gas expands from the throat region to the nozzle exit. For the class of rockets such as the Antares, the flow conditions require the use of a large set of finite rate chemical reactions specific to ammonium perchlorate—aluminum fuel propellants.[16] This set of reactants and rates and the model of thermal nonequilibrium between the gas and the alumina particles are discussed by Kawasaki et al.[4] Figure 3 shows the gas temperature and CO concentration along the nozzle centerline from the throat to the exit obtained with the VIPER model.[4] In Fig. 4 the other major species are shown. The concentrations of NO and OH, potentially strong radiators in the ultraviolet, are seen to be about three orders of magnitude lower than CO. In the nozzle calculations that follow, the conditions shown in Figs. 3 and 4 are used as the bulk flow solution. The CO(a) excitation mechanisms are overlaid on these flow conditions.

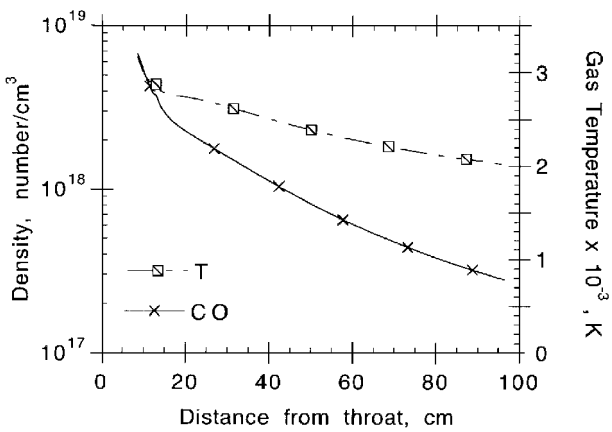

Fig. 3 Nozzle centerline CO concentration and gas temperature.

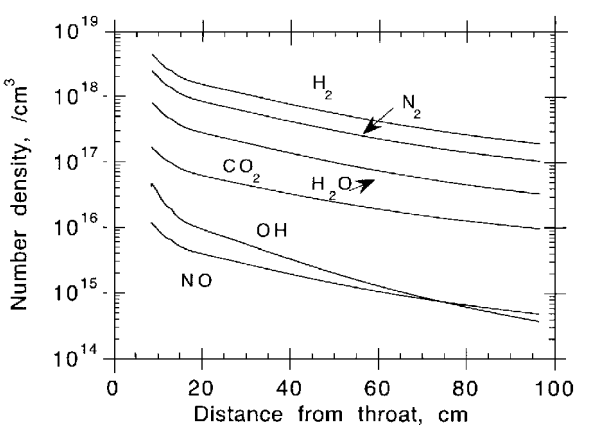

Fig. 4 Nozzle centerline concentrations of other ground-state species.

The CO(a) state is initially created in the combustion chamber at a Boltzmann distribution of about 3,300 K. The state can be deexcited or quenched through neutral collisions or produced by excited state chemical reactions. For the conditions of interest here, the deexcitation by collisional quenching is the most likely process. The quenching of

$$\mathrm{CO}(a), \mathrm{CO}(a) + M \xrightarrow{k_Q} \mathrm{CO}(X) + M$$

has been studied by Slanger and Black[17] and more recently Farrenq and Rossetti.[18] Slanger and Black measured the quenching rate k_Q to be relatively large, 7.6×10^{-11} mol/cm^{3}s, except he noted that the quenching does not occur to the ground vibrational level. The more recent work of Farrenq and Rossetti[18] showed that the state most likely to be populated after a collision is the CO ground state in its 26th vibrational level. Essentially, the electronic energy of the excited CO(a) state is converted into vibrational energy of the ground state. Depending on the number of collisions and the (V-V) and (V-T) rates for removal of CO from its ground electronic and excited vibrational states, the CO(X, $v = 26$) state will be out of equilibrium with the expanding gas. The degree to which this state remains out of equilibrium determines whether the CO(a) formed in the combustion chamber is the source of the radiation observed in flight.

Only a model that retains the manifold of CO ground-state vibrational levels can be used to test this hypothesis. This model can be overlaid with the VIPER solution. To develop such a model we follow closely the work of Chiroux et al.,[19] who considered the rate equations for the individual vibrational states of expanding flows with CO, NO, N_2, and C. The flow that they modeled was assumed to expand through an orifice with an expansion ratio of 110 and initial pressure and temperature of 100 atm and 2000 K, respectively. A number of processes were considered, but those of interest to us are the (V-V), (V-T), and (V-E) rates for excitation and deexcitation of a vibrational manifold of ground state CO and CO(a) in the ground vibrational state. We retain vibrational state specificity for CO(X, $v = 0, 45$) only. The rate equations for CO(a) and CO(X, $v = 0, 45$) are

$$\frac{\mathrm{d}[\mathrm{CO}(a,w)]}{\mathrm{d}t} = -S^{v\to w}\exp\left(-\frac{\Delta E}{kT}\right)[\mathrm{CO}(a,w)][\mathrm{CO}] + S^{v\to w}[\mathrm{CO}(v)][\mathrm{CO}] - A_a[\mathrm{CO}(a,w)] \tag{15}$$

$$\frac{\mathrm{d}[\mathrm{CO}(v)]}{\mathrm{d}t} = (V-V) + (V-T) + (V-E) - A_v[\mathrm{CO}(v)] \tag{16}$$

where S and ΔE are defined by Chiroux et al.[19] and $A_a = 142$ and $A_v = 5$ transitions/s. The basic types of processes considered were

$$\mathrm{CO}(v) + \mathrm{CO}(w-1) \xrightarrow{Q^{v,v-1}_{w-1,w}} \mathrm{CO}(v-1) + \mathrm{CO}(w) \tag{17}$$

$$\mathrm{CO}(v) + X_i \xrightarrow{P^{v,v-1}_{i}} \mathrm{CO}(v-1) + X_i \tag{18}$$

$$\mathrm{CO}(X^1\Sigma, v) + \mathrm{CO}(X^1\Sigma) \xrightleftarrows{S^{v\to w}} \mathrm{CO}(a^3\Pi, w=0) + \mathrm{CO}(X^1\Sigma) \tag{19}$$

Closed-form expressions for the rate coefficients in Eqs. (15–18) from the work of Chiroux et al.[19] were used. Equations (15) and (16) are the source terms [w_s of Eq. (2) for the 46 overlay species]. It was assumed that $\Delta v = \pm 1$ and X_i is CO (in any vibrational level of the ground electronic state). The rate coefficient for the (V-E) expression, Eq. (19), is weighted strongly toward $v = 26$ and $w = 0$ and $v = 19$ and $w = 5$. In addition to Eq. (19), we considered a chemical channel for the formation of CO(a),

$$\mathrm{CO}_2 + \mathrm{C} \leftrightarrow \mathrm{CO}(a) + \mathrm{CO} \tag{20}$$

$$\mathrm{CO}_2 + \mathrm{C} \leftrightarrow \mathrm{CO}(v) + \mathrm{CO}(w) \tag{21}$$

Reactions (19) and (20) were assumed to proceed in both directions, although the forward rate for Eq. (20) remains uncertain.

Figure 5 shows an overlay prediction of the CO ground vibrational state populations for the centerline of the Antares nozzle. The

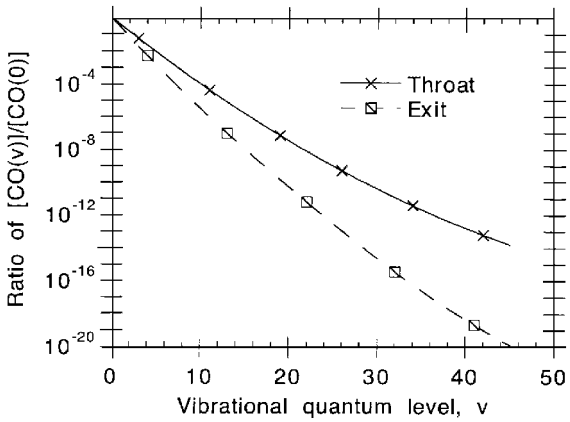

Fig. 5 Distribution of CO vibrational states at the throat and exit plane of the Antares nozzle.

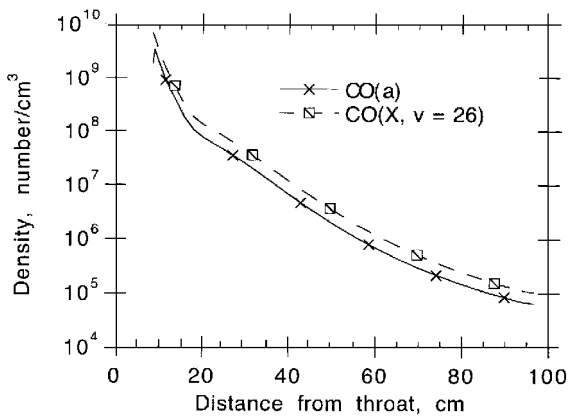

Fig. 6 Profile of CO(a) and CO(X, v=26) along centerline of the Antares nozzle.

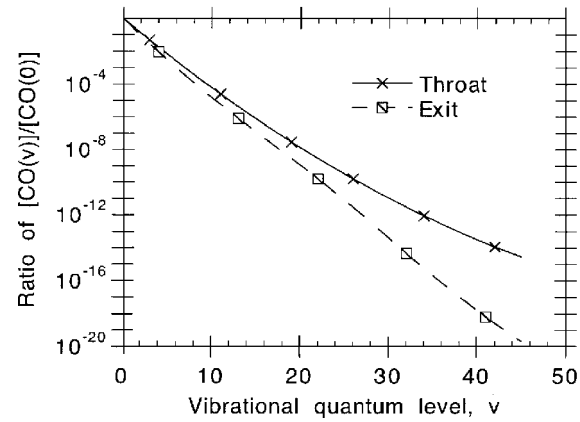

Fig. 7 Distribution of CO vibrational states at the throat and exit plane of the Antares nozzle, chamber pressure reduced by one-tenth.

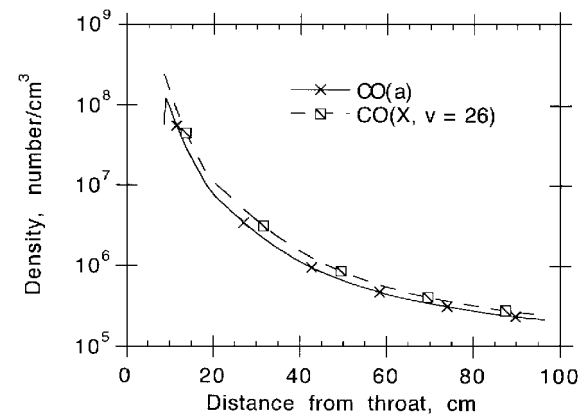

Fig. 8 Profile of CO(a) and CO(X, v = 26) along centerline of the Antares nozzle, chamber pressure reduced by one-tenth.

relative population, CO(X, v)/CO(X, $v = 0$), is shown as a function of vibrational level for the solutions at the throat (top curve) and the nozzle exit plane (lower curve). The throat conditions represent the initial flow conditions determined by the steady-state combustion conditions of 300 psi at a temperature of 3355 K. The curve at the exit deviates somewhat from a Boltzmann distribution. The deviation, however, is not as large as was observed by Chiroux et al.[19] In their case the CO($v = 26$)/CO($v = 0$) ratio at the exit was about 10^{-7} compared with our result of 10^{-13}, for a temperature much less than our gas temperature of about 2100 K. This difference can be explained by the different nozzle characteristics and flow conditions. The Antares nozzle is conical with an expansion ratio of 15.3 instead of 110. The presence of the hot solid particles also sustains the gas temperature to much higher values than the case considered in the work of Chiroux et al.[19] The higher densities and temperatures beyond the throat tend to drive the populations closer to equilibrium conditions in the Antares nozzle. Figure 6 shows the CO(a) and CO(X, $v = 26$) state populations obtained as a function of distance from the throat. The CO(a) state can be seen to closely follow the CO($v = 26$) state population.

During the steady-state burn of the Antares and Star motors the observed spectra was a gray-body continuum superimposed with small molecular features. After the Antares and Star motor burned out, the nature of the spectra changed so that only the Cameron band spectra were observed. The presence of the same molecular radiation during the steady-state burn is inferred from examination of the data.[20] Hence, the overlay-CO populations were also computed with a different bulk solution derived from motor conditions corresponding to a 10-fold reduction in the combustion chamber pressure. Figures 7 and 8 show the CO(X, v) distribution along the nozzle centerline as a function of v and CO(a) vs distance, respectively. Note that the CO(a) number density at the exit is higher than that obtained during nominal motor conditions (see Fig. 6). Reduction of the number density increases the CO vibrational freezing.

The results shown in Figs. 5–8 demonstrate that the overlay technique can be used to model a complex set of kinetics reactions with a large number of states. The use of the model is independent of the nozzle type or operating conditions. The results also evoke the specific question as to whether the degree of freezing is sufficient to explain the observed CO Cameron band emissions. For the nominal operating conditions, the concentration of CO(a) at the exit was computed to be about a factor of 10^3 above that given by equilibrium at the local gas temperature. For the condition where the chamber pressure was reduced (Figs. 7 and 8), the local gas temperature is sufficiently low (1665 K) such that thermally no CO(a) should exist. Consistent with the increase in CO vibrational freezing, we calculate a CO(a) exit concentration of about $2 \times 10^5/\text{cm}^3$. However, with the current model the CO(a) concentration calculated in both cases is insufficient to explain the experimental data by about three orders of magnitude.

We turn to the second class of mechanisms that were considered to test the possibility of producing CO(a) by excitation of nozzle exit species with the plume–body shock layer. The bulk solution for the expanding flow of the rocket exhaust at an altitude of 110 km and speed of 2 km/s was that obtained in earlier work.[6] The calculation of the bulk solution assumed that there are two types of (ground) state gas species present: the gas that leaves the nozzle and the gas that originates in the freestream. Because the densities are low, it is assumed that these two types of gas species do not react with one another. The overlay species considered are CO(a), N_2(A), NO(A), and gaseous C. The concentration of the first three at the start of the external overlay calculation (nozzle exit plane) is determined by the internal nozzle calculation. As was shown, the nozzle exit concentrations of these excited states is small. The initial concentration of C remains a free parameter, to be discussed further.

To calculate the excited state species concentrations the following reactions were considered:

$$CO(a) \xrightarrow{A_a} CO + h\nu \tag{22}$$

$$N_2(A) \xrightarrow{A_{N_2}} N_2 + h\nu \tag{23}$$

$$NO(A) \xrightarrow{A_{NO}} NO + h\nu \tag{24}$$

$$CO(a) + N_2 \xrightarrow{k_{f8}} CO + N_2(A) \tag{25}$$

$$CO(a) + CO \xrightarrow{k_{f9}} 2CO \tag{26}$$

$$N_2(A) + NO \xrightarrow{k_{f10}} N_2 + NO(A) \tag{27}$$

$$CO + N_2(A) \xrightarrow{k_{f11}} CO(a) + N_2 \tag{28}$$

$$2CO \xrightarrow{k_{f12}} CO(a) + CO \tag{29}$$

$$N_2 + NO(A) \xrightarrow{k_{f13}} N_2(A) + NO \tag{30}$$

$$C + O_2 \xrightarrow{k_{f14}} CO(a) + O \tag{31}$$

$$CO(a) + O \xrightarrow{k_{f15}} C + O_2 \tag{32}$$

Table 2 (Ref. 21) provides the values of the rate constants used. Without the inclusions of Eqs. (31) and (32) there was no increase of the CO(a) concentration in the plume shock layer from that at the nozzle exit. Figure 9 shows the spatial dependence of the CO(a) concentration obtained with Eqs. (22–32).

The results shown in Fig. 9 assume an atomic C concentration at the nozzle exit of 10^{13}/cm^3. To obtain agreement with the spectral data,[20] a carbon concentration of 10^{11}/cm^3 is required for the reaction set given by Eqs. (22–32) and the rate coefficient values given in Table 2. This represents a concentration of only one part in 10^7 of the total gas number density. The amount of carbon at the exit plane of solid-propellant exhausts is not well known, although potential sources exist. The internal overlay nozzle calculations showed that the forward and backward reactions of Eqs. (20) and (21) do not account for any carbon formation. Since the Antares motor contains an ablating carbon phenolic throat liner, a source of carbon at the nozzle throat was also assumed in the calculation. Insertion of carbon at the nozzle throat did not produce carbon at the exit because the chemical kinetics are too close to equilibrium. A more likely carbonaceous source at the nozzle exit is from C_2 or C_3. Quantitative modeling of the processes in solid-propellant motors is still needed to establish the number densities for C_2 and C_3 in the nozzle flow. Such species would interact with the freestream O_2 similarly to Eqs. (31) and (32). State specific rates exist,[22] but more measurements are needed to resolve discrepancies in the literature.

Table 2 CO(a) shock layer excitation model rates[a]

Equation no.	C_{fi}	E_{fi}/R
22	1.4×10^5	0.0
23	2.0×10^6	0.0
24	4.7×10^{10}	0.0
25	6.0×10^{12}	2,198.5
26	4.6×10^{13}	0.0
27	3.9×10^{13}	0.0
28	1.2×10^{13}	0.0
29	2.7×10^{14}	70,560.0
30	2.4×10^{14}	9,040.5
31	1.6×10^{13}	0.0
32	1.2×10^{14}	0.0

[a]Nomenclature[21] is as defined in Table 1. The rates are in units of cm^3/mole-s, except for Eqs. (22–24), which are in units of transitions/second. The η terms are all 0.

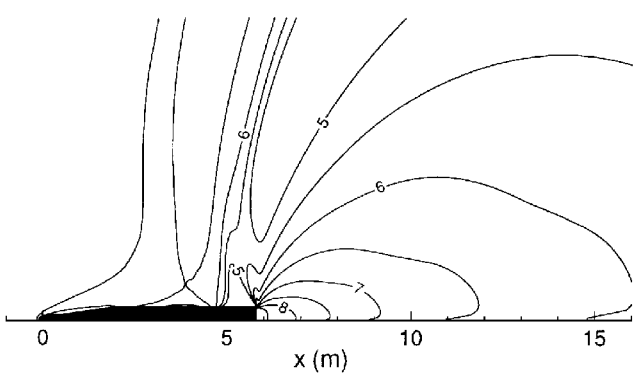

Fig. 9 Contour levels of CO(a) $\log_{10}$(number/cm^3) in the plume of the BSUV2 rocket; 2 km/s and 110-km altitude.

Conclusions

The overlay method has been demonstrated to be an efficient technique in modeling excited state species in compressed and expanding flows. Two different cases have been considered. In the first case, the OH(A) state population has been modeled in the bow shock flow. The population is compared with that derived from the QSS solution. At 85 km differences are apparent, although the radiation at the stagnation point is essentially the same for both models. For the second case that was considered, the computation of the CO(a) state population in a plume flow, the QSS approach is not possible. The efficiency of the method enabled us to study large systems of states, up to 47, for some cases. The approach also permitted us to quantitatively evaluate the contributions from different excited state mechanisms. This study allowed us to conclude that the origin of the Cameron band emission observed during the bow shock ultraviolet flight 2 is most likely due to the interaction of exhaust carbon species such as C_2 or C_3 with freestream atomic oxygen. Although the CO vibrational and electronic a state population is out of equilibrium with the local gas temperature, the degree of nonequilibrium is not sufficient to explain the observed radiation.

Acknowledgments

This research was supported by the Innovative Science and Technology Directorate of the Ballistic Missile Defense Organization (BMDO). Research performed at the Institute for Defense Analyses was carried out under Contract DASW01-94-C-0054 for BMDO.

References

[1]Park, C., "Calculation of Nonequilibrium Radiation in the Flight Regimes of Aero-Assisted Orbital Transfer Vehicles," *Thermal Design of Aero-Assisted Orbital Transfer Vehicles*, edited by H. F. Nelson, Vol. 96, Progress in Astronautics and Aeronautics, AIAA, New York, 1985.

[2]Levin, D., Braunstein, M., Candler, G., Collins, R., and Smith, G., "Examination of Theory for Bow Shock Ultraviolet Rocket Experiments—II," *Journal of Thermophysics and Heat Transfer*, Vol. 8, 1994, p. 453.

[3]Nickerson, G. R., Coates, D. E., Dang, A. L., Dunn, S. S., Berker, D. R., Hermsen, R. L., and Lamberty, J. T., "The Solid Propellant Motor Performance Prediction Computer Program (SPP)," AFAL TR-87-078, Dec. 1987.

[4]Kawasaki, A. H., Dunn, S. S., Coats, D. E., Nickerson, G. R., and Berker, D. R., "Viscous Interaction Performance Evaluation Routine for Two-Phase Nozzle Flows with Finite Rate Chemistry—VIPER," Rept. PL-TR-94-3031, Nov. 1994.

[5]Candler, G. V., and MacCormack, R. W., "The Computation of Hypersonic Ionized Flows in Chemical and Thermal Nonequilibrium," *Journal of Thermophysics and Heat Transfer*, Vol. 5, No. 3, 1991, pp. 266–273.

[6]Candler, G. V., Levin, D. A., Collins, R. J., Erdman, P. W., Zipf, E., Espy, P., and Howlett, C. L., "Comparison of Theory with Plume Radiance Measurements from the Bow Shock Ultraviolet 2 Rocket Flight," *Journal of Thermophysics and Heat Transfer*, Vol. 7, 1993, p. 709.

[7]MacCormack, R. W., and Candler, G. V., "The Solution of the Navier–Stokes Equations Using Gauss-Seidel Line Relaxation," *Computers and Fluids*, Vol. 17, No. 1, 1989, pp. 135–150.

[8]MacCormack, R. W., "Current Status of the Numerical Solution of the Navier–Stokes Equations," AIAA Paper 85-0032, Jan. 1985.

[9]Buning, P. G., and Steger, J. L., "Solution of the Two-Dimensional Euler Equations with Generalized Coordinate Transformations Using Flux-Vector Splitting," AIAA Paper 82-0971, June 1982.

[10]Boyd, I., Candler, G., and Levin, D., "Dissociation Modeling in Low Density Hypersonic Flows of Air," *Physics of Fluids*, Vol. 7, 1995, p. 1757.

[11]Levin, D. A., Candler, G. V., Wright, M., Collins, R. J., and Erdman, P. W., "Examination of OH Ultraviolet Radiation from Shock-Heated Air," *Journal of Thermophysics and Heat Transfer*, Vol. 10, 1996, pp. 200–208.

[12]Baulch, D. L., Drysdale, D. D., Home, D. G., and Lloyd, A. C., *Evaluated Kinetic Data for High Temperature Reactions, 1, Homogeneous Gas Phase Reactions of the H_2-O_2 System*, Butterworths, London, 1972.

[13]Hidaka, Y., Takahashi, S., Kawano, H., Suga, M., and Gardiner, W. C., "Shocktube Measurements of the Rate Constant for Excited OH($A^2\Sigma^+$) Formation in the Hydrogen-Oxygen Reaction," *Journal of Physical Chemistry*, Vol. 86, 1982, pp. 1429–1433.

[14]Davis, M. G., McGregor, W. K., and Mason, A. A., "OH Chemiluminescent Radiation from Lean Hydrogen-Oxygen Flames," *Journal of Chemical Physics*, Vol. 61, No. 4, 1974, pp. 1352–1356.

[15]Copeland, R. A., Wise, M. L., and Crosely, D. R., "Vibrational Energy Transfer and Quenching of OH($A^2\Sigma^+$, $v\prime = 1$)," *Journal of Physical Chemistry*, Vol. 92, No. 20, 1988, pp. 5710–5715.

[16]Anon., "Manufacturer's Data," Hercules, Inc., Cumberland, MD, 1966.

[17]Slanger, T. G., and Black, G., "CO($a^3\Pi$), Its Production, Detection, Deactivation, and Radiative Lifetime," *Journal of Chemical Physics*, Vol. 55, 1971, p. 2164.

[18]Farrenq, R., and Rossetti, C., "Vibrational Distribution Functions in a Mixture of Excited Isotopic CO Molecules," *Chemical Physics*, Vol. 92, 1985, pp. 401–416.

[19]Chiroux de Gavelle de Roany, A., Flament, C., Rich, J. W., Subramaniam, V. V., and Warren, W. R., "Strong Vibrational Nonequilibrium in Supersonic Nozzle Flows," *AIAA Journal*, Vol. 31, No. 1, 1993, pp. 119–128.

[20]Erdman, P. W., Zipf, E. C., Espy, P., Howlett, C., Christou, C. T., Levin, D. A., Collins, R. J., and Candler, G. V., "In-Situ Measurements of UV Plume Radiation from the Bow Shock Ultraviolet 2 Rocket Flight," *Journal of Thermophysics and Heat Transfer*, Vol. 7, 1993, p. 704.

[21]Schofield, K., "Critically Evaluated Rate Constants for Gaseous Reactions of Several Electronically Excited Species," *Journal of Physical and Chemical Reference Data*, Vol. 8, No. 3, 1979, pp. 723–796.

[22]Reisler, H., Mangir, M., and Wittig, C., "The Kinetics of Free Radicals Generated by IR Laser Photolysis. II. Reactions of $C_2(X^1\Sigma_g^+)$, $C_2(a^3\Pi_u)$, $C_3(X^1\Sigma_g^+)$, and CN($X^2\Sigma^+$) with O_2," *Chemical Physics*, Vol. 47, 1980, pp. 49–58.